

# A lattice formulation of Weyl fermions on a single curved surface

Shoto Aoki, Hidenori Fukaya, and Naoto Kan

*Department of Physics, Osaka University, Toyonaka 560-0043, Japan*

.....  
 In the standard lattice domain-wall fermion formulation, one needs two flat domain-walls where both of the left- and right-handed massless modes appear. In this work we investigate a single domain-wall system with a nontrivial curved background. Specifically we consider a massive fermion on a  $3D$  square lattice, whose domain-wall is a  $2D$  sphere. In the free theory, we find that a single Weyl fermion is localized at the wall and it feels gravity through the induced spin connection. With a topologically nontrivial  $U(1)$  link gauge field, however, we find a zero mode with the opposite chirality localized at the center where the gauge field is singular. In the latter case, the low-energy effective theory is not chiral but vectorlike. We discuss how to circumvent this obstacle in formulating lattice chiral gauge theory in the single domain-wall fermion system.

arXiv:2402.09774v3 [hep-lat] 21 May 2024

# 1 Introduction

Lattice gauge theory has been successful in understanding and computing nonperturbative dynamics of particle physics. Numerical simulation of quantum chromodynamics (QCD) on a flat Euclidean lattice has been an essential tool for examining the standard model in various hadronic processes. Domain-wall fermions, in particular, defined on a five-dimensional square lattice, achieve a good control of chiral symmetry, where the unwanted mixing between the left- and right-handed quarks is well suppressed.

In the standard domain-wall fermion formulation [1–3] on a flat five-dimensional lattice, we need at least two domain-walls where the left- and right-handed massless fermions are localized. If one of them is decoupled from the gauge fields, the system may enable formulation of a chiral gauge theory on a lattice [4–7]<sup>1</sup>. In order to decouple the unwanted modes, a smooth elimination of gauge fields has been considered in [11, 12] but it turned out that this task is not that easy. For instance, the cobordism invariance of the instanton background forces the two domain-walls to have the same number of zero modes [13] (see also related works [14–17]). This indicates that the low energy theory has both of the left- and right-handed modes. Another approach is the so-called symmetric mass generation [18–31], which gaps out the unwanted chiral modes by generating mass without breaking the chiral symmetry. This, however, requires a highly nonperturbative dynamics.

In our recent works [32, 33] we have been studying a massive fermion system with a non-flat single domain-wall. In the case with an  $S^1$  domain-wall embedded into a flat  $2D$  square lattice, we observed that massless Dirac fermion appears on the wall, having a definite eigenvalue of the gamma matrix perpendicular to the domain-wall. Similarly, we observed that a two-flavor massive fermion, which respects the time-reversal symmetry, yields a massless Dirac fermion on the  $S^2$  domain-wall embedded in flat three dimensions. Also in this case, the edge-localized modes are the eigenstates of the gamma matrix accompanied by an operator exchanging the flavor index.

Moreover, it was found through the Dirac operator spectrum that the edge-localized modes feel gravity via the induced spin connection on the curved domain-wall. This is a realization of the Einstein equivalence principle, which tells that any acceleration is indistinguishable from gravity. We have numerically confirmed that the rotational symmetry is monotonically recovered toward the classical continuum limit of the higher-dimensional square lattice. The limit of the Dirac operator eigenvalue spectrum is consistent with that in

---

<sup>1</sup> Instead of directly using the domain-wall fermions, the effective four-dimensional Dirac operator or known as the overlap Dirac operator [8] was used to formulate some successful examples of nonperturbative formulation of lattice chiral gauge theory. See Refs. [7, 9, 10] and the references therein.

the continuum theory, which has a manifest gauge symmetry under the general coordinate transformation.

In this work, we extend our study on the curved domain-wall fermions in two new directions. One is to employ Shamir's formulation [2, 3]. We consider a  $2D$  spherical domain-wall embedded into a  $3D$  square lattice, but we ignore the lattice points outside of the domain-wall, which is equivalent to taking the fermion mass to  $+\infty$ . The second is to consider a single-flavor fermion, which loses the time-reversal symmetry in three dimensions. Then the edge-localized modes should represent not Dirac but Weyl fermions. From the Dirac operator spectrum, we investigate the gravity induced on the wall, and examine its continuum limit. A preliminary result of this work was presented in Ref. [34].

In this setup, a single massless fermion with a definite chirality is localized on a single domain-wall. Namely, it looks as if a Weyl fermion on an  $S^2$  surface is nonperturbatively regularized on a lattice. In recent publications [35, 36] this single-domain-wall system was proposed as a lattice regularization of chiral gauge theories.

Contrary to the expectation, when it is coupled to the  $U(1)$  gauge field, we observe a nontrivial dynamics where the low-energy theory becomes not chiral but rather vectorlike. This happens when the gauge field on the  $S^2$  has a nontrivial topological charge. The Gauss law in three dimensions requires a singular source of the gauge flux inside the spherical domain-wall. This configuration is an analog of a magnetic monopole in three spatial dimensions, whose magnetic flux penetrates the  $S^2$  surface. The additive mass renormalization through the Wilson term due to the singular gauge field becomes strong enough to flip the sign of the effective mass of the fermion, and another domain-wall is created around the singularity. The dynamically created domain-wall captures a single fermion zero mode with the opposite chirality to the original edge modes on the  $S^2$ . This dynamical creation of domain-walls was already reported in our previous work on the Dirac fermion system [37, 38] which gives a microscopic description of the Witten effect [39]: the magnetic monopole gains an electric charge because the electron zero mode is bound to the small but finite spherical domain-wall around the monopole. We discuss how to circumvent this obstacle in formulating chiral gauge theory.

The rest of this paper is organized as follows. In Sect. 2 we show that the edge-localized modes generally exist and they feel the induced gravity. In Sect. 3 we analyze the lattice domain-wall fermion system numerically. Our result shows that a Weyl fermion appears on the  $S^2$  domain-wall, as is expected. In Sect. 4, however, we show that an oppositely chiral zero mode appears when the gauge field has a point-like singularity. We discuss in Sect. 5 how to avoid the unwanted zero modes with the opposite chirality. A summary is given in Sect. 6.

## 2 Continuum analysis of 3D dimensional Shamir domain-wall fermion with a single $S^2$ boundary

We first consider a Dirac fermion action in a 3D flat continuum spacetime  $\mathbb{R}^3$ ,

$$S = \int d^3x \bar{\psi} D \psi(x), \quad (1)$$

where the Dirac operator with a position-dependent mass  $m(x)$  is given by

$$D = \sum_{i=1}^3 \sigma^i \left( \frac{\partial}{\partial x^i} - i A_i(x) \right) + m(x). \quad (2)$$

Here we have introduced a background  $U(1)$  gauge field  $A_i(x)$  and  $\sigma^i$  denote the Pauli matrices representing the gamma matrices in three dimensions.

We assume that the mass function  $m(x)$  has a spherical domain-wall structure:

$$m(x) = \begin{cases} -m & \text{for } |x| \leq r_0 \\ +M & \text{otherwise} \end{cases}, \quad (3)$$

where we assume  $m > 0, M > 0$ . In order to obtain the Shamir domain-wall fermion Dirac operator, we take the  $M \rightarrow +\infty$  limit, which is equivalent to imposing a boundary condition

$$\sigma_r \psi(x) = +\psi(x) \quad \text{at } |x| = r_0. \quad (4)$$

Here the chirality operator  $\sigma_r$  is given by

$$\sigma_r = \frac{\sum_i \sigma^i x_i}{|x|}, \quad (5)$$

which is well-defined at any point on the  $S^2$  surface  $|x| = r_0$ . In the same way, the conjugate operator  $D^\dagger$  requires the boundary condition with the opposite chirality  $\sigma_r = -1$ .

We show below that the chiral edge-localized modes generally exist on the curved spherical domain-wall, at least approximately in Sect. 2.1. We also derive in Sect. 2.2 an exact eigenfunction when the gauge field configuration respects the rotational symmetry.

### 2.1 Edge-localized modes in general background gauge field

First, let us confirm the existence of the edge-localized modes in a general  $U(1)$  gauge field background. Here we assume that the gauge field is smooth everywhere without any singularity.

In the polar coordinates and taking the radial gauge condition  $A_r = 0$ , the Dirac operator inside the domain-wall  $|x| \leq r_0$  is expressed by

$$D = \sigma_r \left( \frac{\partial}{\partial r} + \frac{1}{r} - \frac{r_0}{r} iD^{S^2} \right) - m, \quad (6)$$

where the Hermitian operator  $iD^{S^2}$  is defined by

$$iD^{S^2} := \frac{1}{r_0} \left( 1 - i\sigma_2 \exp(i\phi\sigma_3) \left( \frac{\partial}{\partial \theta} - i\hat{A}_\theta \right) - \frac{1}{\sin \theta} \sigma_r \sigma_2 \exp(i\phi\sigma_3) \left( \frac{\partial}{\partial \phi} - i\hat{A}_\phi \right) \right). \quad (7)$$

Here we have introduced the dimensionless vector potentials:  $\hat{A}_\theta := rA_\theta$  and  $\hat{A}_\phi := r \sin \theta A_\phi$ .

In fact, we can identify  $D^{S^2}$  as the effective Dirac operator on  $S^2$  for the low-energy edge-localized modes. Taking a gauge transformation or the Euclidean version of the local Lorentz transformation,

$$R(\theta, \phi) = \exp(i\theta\sigma^2/2) \exp(i\phi\sigma^3/2), \quad (8)$$

as well as a  $U(1)$  gauge transformation, we obtain the  $2D$  massless Dirac operator:

$$e^{-i\frac{\phi}{2}} R(\theta, \phi) iD^{S^2} e^{i\frac{\phi}{2}} R(\theta, \phi)^{-1} = -\frac{1}{r_0} \sigma_3 \left[ \sigma_1 \left( \frac{\partial}{\partial \theta} - i\hat{A}_\theta \right) + \frac{\sigma_2}{\sin \theta} \left( \frac{\partial}{\partial \phi} - i\hat{A}_\phi + \frac{i}{2} - \frac{i \cos \theta}{2} \sigma_3 \right) \right]. \quad (9)$$

We can see that the spin connection  $\sigma_3 \cos \theta/2$  is induced<sup>2</sup>. It is also important to note that the rotated  $2D$  Dirac operator anticommutes with the chirality operator  $R(\theta, \phi) \sigma_r R(\theta, \phi)^{-1} = \sigma_3$ .

Let  $\chi(\theta, \phi)$  be a function in the domain of  $iD^{S^2}$  at  $r = r_0$ . Then we can construct an edge-localized mode

$$\psi_+^e = \frac{1}{r} \exp[-m(r_0 - r)] P_+ \chi(\theta, \phi), \quad (10)$$

in relation to which the Dirac operator effectively acts as

$$D = P_- (iD^{S^2}) P_+, \quad (11)$$

with the chiral projection operators  $P_\pm := (1 \pm \sigma_r)/2$ . Here we have used an approximation in the large  $m$  limit,

$$\frac{1}{r} iD^{S^2} \exp[-m(r_0 - r)] \sim \frac{1}{r_0} iD^{S^2} \exp[-m(r_0 - r)]. \quad (12)$$

Thus, the edge-localized mode  $\psi_+^e$  represents one massless fermion with positive chirality on the single  $S^2$  surface with radius  $r_0$ .

---

<sup>2</sup>To be precise, the induced connection is spin-c with an additional  $U(1)$  part  $\frac{i}{2}$ , which, however, can be eliminated by the gauge transformation. We keep this unphysical  $U(1)$  part nonzero to make the analysis simpler, since otherwise, the gauge transformation requires multiple-patch covering of  $\mathbb{R}^3$  to avoid multivaluedness of the gauge transformation with respect to  $\theta$ .

When we take  $M$  in Eq. (3) to negative infinity keeping the sign of  $m$  unchanged, the boundary condition requires the negative chirality at  $r = r_0$ , which prohibits the edge-localized modes. If we take both  $m$  and  $M$  negative, the negatively chiral edge-mode

$$\psi_-^e = \frac{1}{r} \exp[m(r_0 - r)] P_- \chi(\theta, \phi), \quad (13)$$

appears. The case with  $mM < 0$  is analogous to a normal insulator where no edge-localized mode appears, and  $mM > 0$  corresponds to a topological insulator where the existence of the edge excitation is topologically protected. Thus, our curved domain-wall fermion system with  $mM > 0$  has the edge-localized modes, which describe a single Weyl fermion on a single curved surface.

The edge-localized Weyl fermion feels inertial force resulting from the constrained motion. As explicitly shown in Eq. (9), this force can be identified as gravity through the induced spin connection. This is consistent with Einstein's equivalence principle, which indicates that any constraint force can be identified as gravity. Since the edge modes are constrained on the curved  $S^2$  surface, gravity is naturally induced on them. Interestingly, the induced gravity reflects only intrinsic geometry and the extrinsic information is invisible. This is not special for  $S^2$  but true on general curved domain-walls as discussed in Ref. [40]. The extrinsic curvature contribution is suppressed exponentially in the large- $m$  limit.

## 2.2 Exact edge-localized modes with rotational symmetry

Next we exactly solve the eigenproblem of the curved domain-wall fermion Dirac operator in the case where the system has a rotational symmetry. Let us take the radial gauge  $A_r = 0$  and assume that the field strength  $F_{\mu\nu}$  perpendicular to the domain-wall is uniformly distributed. Such  $U(1)$  backgrounds are classified by the topological charge,

$$n = \frac{1}{4\pi} \int_{S^2} d^2x \epsilon^{\mu\nu} F_{\mu\nu}, \quad F_{12} = -F_{21} = \frac{n}{2r_0^2}. \quad (14)$$

Our target gauge field background in the whole  $3D$  space is achieved by putting a ‘‘monopole’’ at the origin<sup>3</sup>. The vector potential generated by the monopole is

$$A_1 = \frac{-q_m y}{r(r+z)}, \quad A_2 = \frac{q_m x}{r(r+z)}, \quad A_3 = 0, \quad (15)$$

where  $q_m$  is the magnetic charge of the monopole, which satisfies the Dirac's quantization condition  $q_m = \frac{n}{2}$  ( $n \in \mathbb{Z}$ ). To be precise, this expression has a singularity at  $x = y = 0$

---

<sup>3</sup>It may not be adequate to name this configuration a ‘‘monopole’’ since our gauge potential is considered not in  $3D$  space but in  $2 + 1$ -dimensional spacetime. But the computation is completely parallel to the case with the monopole in three spatial dimensions we discussed in Ref. [37].

and  $z < 0$ , which is the so-called Dirac string. In order to eliminate the Dirac string, we need another set of the gauge potentials in the  $z \leq 0$  region but here we simply ignore the neighborhood of the string. In fact, the Dirac string automatically disappears in the lattice regularization that we will discuss in the next section. The field strength we have obtained is

$$F_{ij} = \partial_i A_j - \partial_j A_i = q_m \epsilon_{ijk} \frac{x_k}{r^3}. \quad (16)$$

With the above spherically symmetric gauge field background, the effective 2D Dirac operator  $iD^{S^2}$  can be written as

$$D^{S^2} = \frac{1}{r_0} \left[ \sigma^i \left( L_i + n \frac{x_i}{2r} \right) + 1 \right], \quad (17)$$

where  $L_i$  is the orbital angular momentum operator in the presence of the monopole,

$$L_i = -i \epsilon_{ijk} x^j \left( \frac{\partial}{\partial x^k} - i A_k \right) - n \frac{x_i}{2r}. \quad (18)$$

Instead of  $D$  itself, let us solve the eigenproblem of the Hermitian operator  $D^\dagger D$ . Note that  $D^\dagger D$  commutes with the total angular momentum operators  $J^i = L^i + \sigma^i/2$  as well as  $D^{S^2}$  so that it is convenient to consider the simultaneous eigenstates of  $\mathbf{J}^2 = \sum_i (J^i)^2$ ,  $J^3$  and  $D^{S^2}$ . Let  $j$  be the highest weight of  $\mathbf{J}$ , which takes discrete values<sup>4</sup>

$$j = \frac{|n| - 1}{2}, \frac{|n| - 1}{2} + 1, \frac{|n| - 1}{2} + 2 \cdots, \quad (19)$$

with a constraint  $j \geq 0$ . The eigenfunction denoted by  $\chi_{j,j_3,\pm}$  satisfies

$$\mathbf{J}^2 \chi_{j,j_3,\pm} = j(j+1) \chi_{j,j_3,\pm}, \quad (20)$$

$$J_3 \chi_{j,j_3,\pm} = j_3 \chi_{j,j_3,\pm}, \quad (21)$$

$$iD^{S^2} \chi_{j,j_3,\pm} = \pm \frac{\nu}{r_0} \chi_{j,j_3,\pm}, \quad \nu = \sqrt{\left( j + \frac{1}{2} \right)^2 - \frac{n^2}{4}}, \quad (22)$$

$$\sigma_r \chi_{j,j_3,\pm} = \chi_{j,j_3,\mp}. \quad (23)$$

Here we have used facts that  $(D^{S^2})^2$  is written as a linear combination of  $\mathbf{J}^2$ ,  $\sigma_r$  and identity, and that  $D^{S^2}$  anticommutes with  $\sigma_r$ . As will be shown below, the edge-localized eigenvalue of  $D^\dagger D$  depends only on  $j$ . Therefore the degeneracy of the eigenvalue is  $2(2j+1)$  [37, 41].

---

<sup>4</sup>The lower bound of  $j$  comes from the nontrivial contribution from monopole, which is proportional to  $n$ .

Since the chirality operator  $\sigma_r$ , which determines the boundary condition at  $r = r_0$ , anticommutes with  $D^{S^2}$ , the eigenstate  $\psi$  of  $D^\dagger D$  is written by a linear combination of  $\chi_{j,j_3,\pm}$ :

$$\psi = \frac{1}{\sqrt{r}} [g_+(r)\chi_{j,j_3,+} + g_-(r)\chi_{j,j_3,-}]. \quad (24)$$

Substituting this into the equation  $D^\dagger D\psi = E^2\psi$ , where we assume  $m^2 > E^2$ , we find that the functions  $g_\pm(r)$  satisfy the modified Bessel equations with a rescaled variable  $z = \kappa r$  where  $\kappa = \sqrt{m^2 - E^2}$ ,

$$\left[ \frac{\partial^2}{\partial z^2} + \frac{1}{z} \frac{\partial}{\partial z} - \frac{(\nu \mp 1/2)^2}{z^2} - 1 \right] g_\pm = 0. \quad (25)$$

From the regularity condition at  $r = 0$ , we find the solutions in terms of the modified Bessel function of the first kind:  $g_+(r) = AI_{\nu-1/2}(\kappa r)$  and  $g_-(r) = BI_{\nu+1/2}(\kappa r)$  with numerical constants  $A$  and  $B$ , respectively. Since  $I_\mu(z)$  are an exponentially increasing function of  $z$ , the solutions are exponentially localized at the edge,  $r = r_0$ .

The boundary condition at  $r = r_0$ :  $\sigma_r\psi = +\psi$  and  $\sigma_r D\psi = -D\psi$  leads to two equations

$$AI_{\nu-1/2}(\kappa r_0) = BI_{\nu+1/2}(\kappa r_0), \quad (26)$$

$$(\kappa B - mA)I_{\nu-1/2}(\kappa r_0) = -(\kappa A - mB)I_{\nu+1/2}(\kappa r_0), \quad (27)$$

which determine the coefficients  $A, B$  up to normalization, and the eigenvalue  $E^2$ . According to the asymptotic form  $I_\mu(z) \sim \frac{e^z}{\sqrt{2\pi z}} \left(1 - \frac{4\mu^2 - 1}{8z}\right)$ , the eigenvalue converges to

$$E^2 = \frac{\nu^2}{r_0^2} \quad (28)$$

in the large- $\kappa r_0$  limit, which is independent of the mass parameter  $m$ . Moreover, the eigenvalue is shared with that of the massless 2D Dirac operator  $(iD^{S^2})^2$  shown in Eq. (22). It is important to remark in the free case with  $n = 0$  that the eigenvalue is gaped from zero, which is a gravitational effect [32, 42].

The case of  $j = \frac{|n|-1}{2}$  with  $n \neq 0$ , is qualitatively different from the above result. Let  $\chi_{j,j_3,0}$  be an eigenstate satisfying

$$\mathbf{J}^2 \chi_{j,j_3,0} = j(j+1)\chi_{j,j_3,0} \quad (29)$$

$$J_3 \chi_{j,j_3,0} = j_3 \chi_{j,j_3,0} \quad (30)$$

$$iD^{S^2} \chi_{j,j_3,0} = 0 \quad (31)$$

$$\sigma_r \chi_{j,j_3,0} = \text{sign}(n)\chi_{j,j_3,0}. \quad (32)$$



Assuming the edge-localized mode has the following form,

$$\psi_0 = \frac{1}{\sqrt{r}} f(r) \chi_{j,j_3,0}, \quad (33)$$

we find that  $f(r)$  satisfies the same equation as Eq. (25), but with  $\nu = 0$  and thus we obtain

$$f(r) = C I_{1/2}(\kappa r) = C \sqrt{\frac{2}{\pi \kappa r}} \sinh(\kappa r), \quad (34)$$

with a normalization constant  $C$ .

It is interesting to note that the chiral boundary condition  $\sigma_r \psi_0(r = r_0) = +\psi_0(r = r_0)$  is never satisfied with  $n < 0$ . Also, another boundary condition  $\sigma_r D\psi_0(r = r_0) = -D\psi_0(r = r_0)$  is only satisfied by  $D\psi_0(r = r_0) = 0$  when we take the  $m \rightarrow \infty$  limit. This reflects the Atiyah-Singer (AS) index theorem [43] on the sphere  $S^2$ ,

$$\text{Ind} D^{S^2} = \frac{1}{4\pi} \int_{S^2} d^2x e^{\mu\nu} F_{\mu\nu} = n. \quad (35)$$

The Weyl fermion with positive chirality cannot give a negative contribution to the index when  $n < 0$ . Only in the  $m \rightarrow \infty$  limit do we have an exactly chiral zero mode of both  $D^\dagger D$  and  $iD^{S^2}$ .

Thus, we have obtained the exact massless edge-localized modes with the positive chirality, describing a Weyl fermion on the sphere with radius  $r_0$ . Their existence is guaranteed even in the presence of nontrivial gauge field background. This single domain-wall fermion system looks a good candidate for nonperturbatively formulating chiral gauge theory on a lattice. Note, however, that the chirality is not perfect unless we take the  $mr_0 \rightarrow \infty$  limit. In particular, it is not obvious in the above analysis what will happen to the chiral zero mode when  $mr_0$  is finite. So far we have ignored the short-distance singularity at the location of the monopole. As will be seen below, a highly nonperturbative and careful short-distance analysis is needed to understand this problem.

### 3 Lattice analysis in free theory

In this section we discuss a lattice regularization of the curved domain-wall fermion system. In the free fermion theory with trivial link variables we show that a single Weyl fermion appears on a single spherical domain-wall. We also discuss its continuum and finite volume systematics.

For discretization of the Dirac operator, we employ the Wilson Dirac operator

$$D_W = \sum_{i=1}^3 \sigma^i \frac{\nabla_i - \nabla_i^\dagger}{2a} + \sum \frac{w}{2a} \nabla_i \nabla_i^\dagger - m, \quad (36)$$

where the lattice spacing is denoted by  $a$ , and we assume that  $m > 0$ . The difference operator in the  $i$ -direction for a spinor field located at the lattice site  $x$  is defined by

$$(\nabla_i \psi)_x = \psi_{x+\hat{i}} - \psi_x, \quad (37)$$

with the unit vector  $\hat{i}$  in the corresponding direction. As the standard choice, we take the coefficient of the Wilson term  $w = 1$ . With this choice, the Dirac operator can be written as

$$D_W = -\frac{1}{a} \sum_{i=1}^3 \left( P_-^i \nabla_i + P_+^i \nabla_i^\dagger \right) - m, \quad P_\pm^i = \frac{1 \pm \sigma_i}{2}. \quad (38)$$

It was shown by Shamir [2] in the standard flat domain-wall fermion that there is no need to impose a chiral boundary condition on the lattice but it is enough to simply to set  $\psi_x = 0$  outside the domain-wall. The same is true for our curved case. As shown in Fig. 1 where a  $2D$  slice at  $z = 1/2$  is drawn, we impose

$$\psi_x = 0 \quad \text{if } |x - x_0| \geq r_0, \quad (39)$$

where the center of the domain-wall is put at the origin  $x_0 = (0, 0, 0)$ . Note that our lattice sites are put at half-integral points:  $x = ((2n_1 - 1)/2, (2n_2 - 1)/2, (2n_3 - 1)/2)$  with integer values  $n_i$ . Put  $x$  be one of the inner nearest-neighbor sites of the domain-wall, where  $x + \hat{j}$  is put outside of the wall. Then the Dirac operator acts as

$$(D_W \psi)_x = -\frac{1}{a} \left[ P_-^j (-\psi_x) - P_+^j (\psi_x - \psi_{x-\hat{j}}) \right] + \dots \quad (40)$$

which imposes the boundary condition  $P_-^j \psi_x = 0$  in the continuum limit  $a \rightarrow 0$ , while  $P_+^j \psi_x$  can be taken arbitrarily, as far as  $\psi_x - \psi_{x-\hat{j}} \sim O(a)$ . With this simple boundary condition, the Hermitian conjugate of the Wilson Dirac operator  $D_W^\dagger$  is canonically defined.

To be precise, our domain-wall is not a smooth sphere but a rather digitized zig-zag surface like a block toy as depicted in Fig. 1. It is, therefore, important to check if the rotational symmetry is recovered in the continuum limit. In our previous work on Dirac fermions [42], we already obtained positive numerical evidence. The rotational symmetry of the lowest eigenmodes was almost linearly recovered in the  $a \rightarrow 0$  limit. We will address this issue for the Weyl fermion at the end of this section.

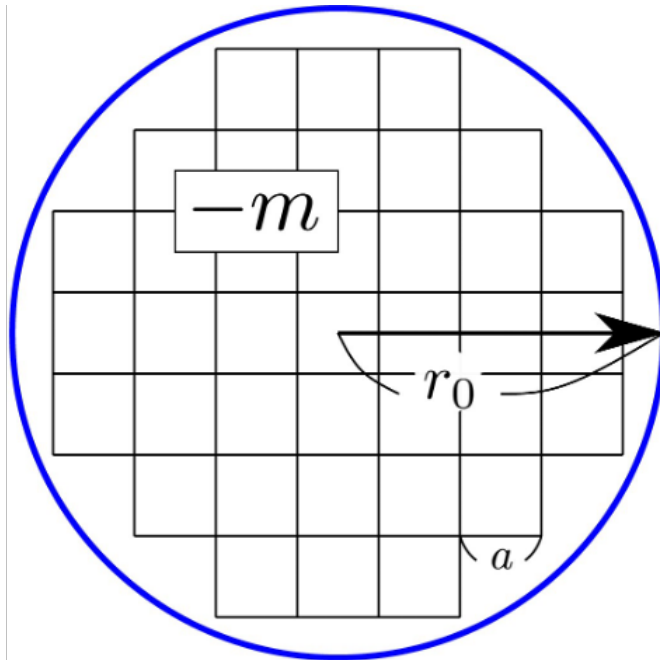


**Fig. 1** A 2D slice at  $z = 1/2$  of the spherical domain-wall in our lattice space. The hopping to the outside of the sphere  $r = r_0$  is cut off. Adapted from [34].

We numerically solve the eigenproblem of  $D_W^\dagger D_W$  as well as  $D_W D_W^\dagger$  which are both Hermitian. With the obtained normalized eigenfunction  $\phi_k(x)$ , where  $k$  is the label for the low-lying modes, we measure the expectation value

$$\sum_x \phi_k^\dagger(x) \sigma_r(x) \phi_k(x), \quad (41)$$

where the chirality operator  $\sigma_r(x) = \sum_i \sigma_i x^i / |x|$  is unambiguously defined at all our half-integral lattice sites. We also scan the local chirality, defined by

$$\phi_k^\dagger(x) \sigma_r(x) \phi_k(x) / \phi_k^\dagger(x) \phi_k(x), \quad (42)$$

for each lattice site  $x$  in order to study its spatial distribution. This turns out to be useful in analyzing the case with a nontrivial  $U(1)$  gauge field background in the next section.

In Fig. 2, we plot the eigenvalue spectrum of  $D_W^\dagger D_W$  at  $r_0 = 24a$  and  $ma = 0.35$ . Solving  $D_W^\dagger D_W \phi_k = E_k^2 \phi_k$ , its square root normalized by  $r_0$ :  $r_0 |E|$  is plotted by filled circle symbols. The color gradation shows the chirality expectation value. We can see that the low-lying modes below  $mr_0$ , shown by the dotted horizontal line, have the positive chirality. The obtained eigenvalues agree with the continuum prediction marked by cross symbols in which the finite volume correction to the infinite volume value  $r_0 |E| = \nu = 1, 2, 3, \dots$  in Eq. (28)

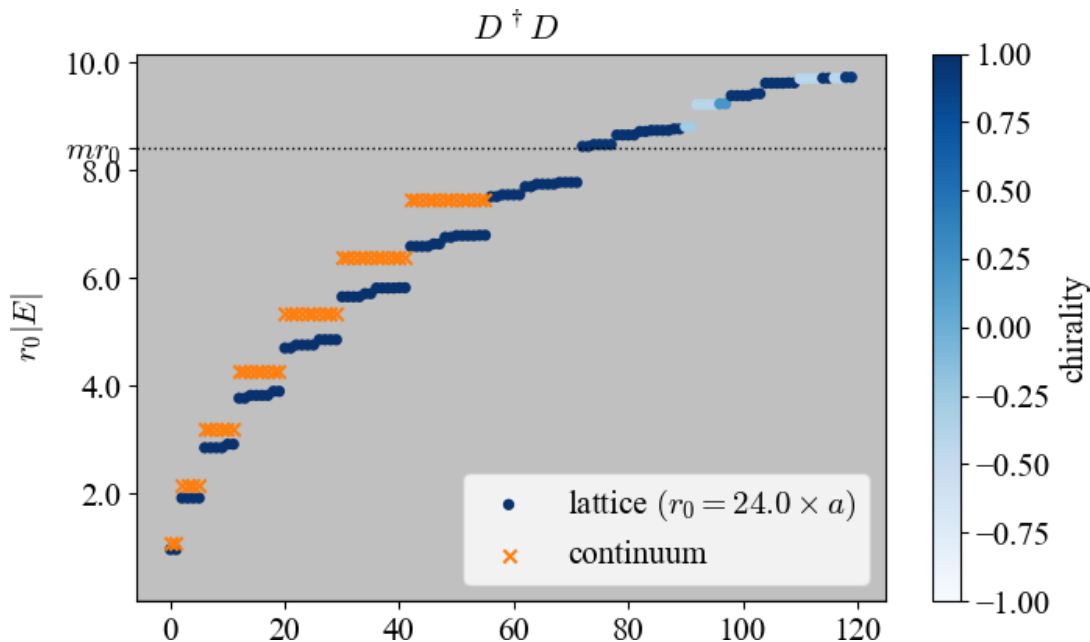


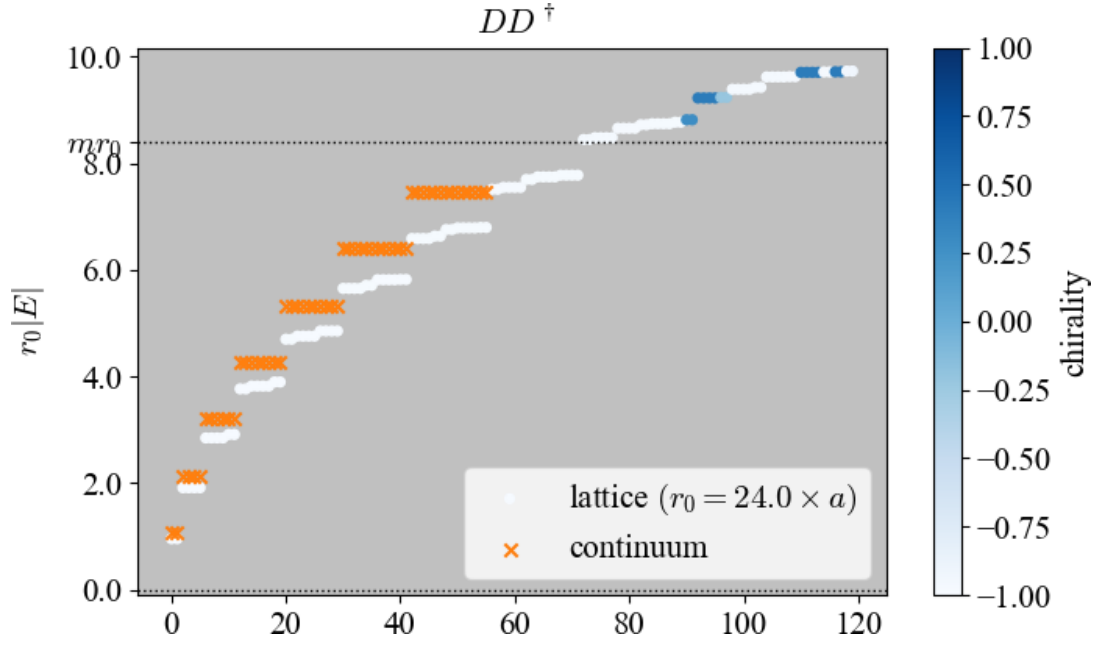
**Fig. 2** The spectrum of  $D_W^\dagger D_W$  at  $r_0 = 24a$  and  $ma = 0.35$ . The square-rooted value  $r_0|E|$  is plotted. The color gradation shows the chirality expectation value. The dotted horizontal line indicates the value of mass  $mr_0$ , above which the eigenmodes are extended to the bulk. Our low-lying eigenvalues below  $mr_0$  of the edge-localized modes agree well with the continuum prediction marked by cross symbols.

is taken into account. The  $2(j + 1/2)$  (or  $2\nu$  in this case) degeneracy with  $j = 1/2, 3/2, \dots$  looks also consistent. The gravitational effect through the induced spin connection, or the gap from zero is clearly seen.

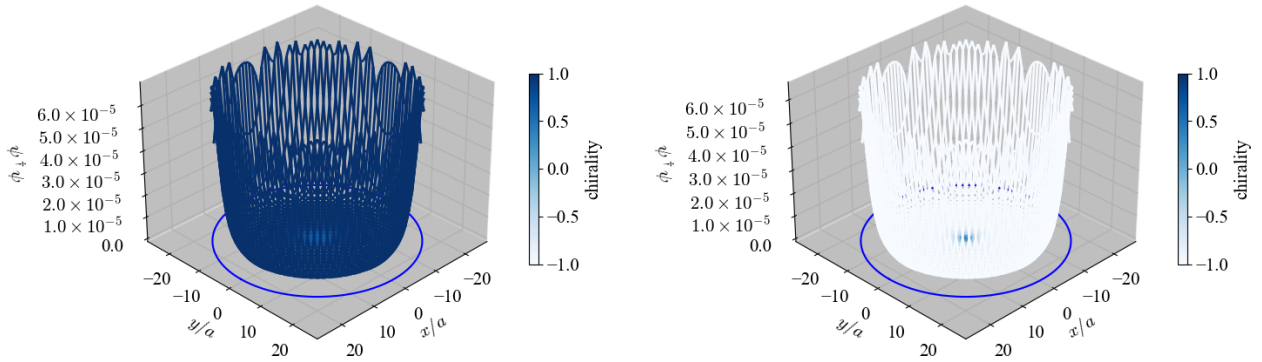
We also plot the eigenvalue spectrum of  $D_W D_W^\dagger$  on the same lattice at Fig. 3. The spectrum is the same as that of  $D_W^\dagger D_W$  but the chirality is opposite.

Figure 4 presents the amplitude of the lowest eigenmode at the  $z = 1/2$  slice of  $D_W^\dagger D_W$  (left panel) and that of  $D_W D_W^\dagger$  (right). The color gradation indicates the local chirality defined by Eq. (42). As is expected, these eigenmodes are localized at the domain-wall  $r = r_0$  and have a uniform distribution of the chirality.

In order to estimate the systematic error due to the lattice discretization, we vary the lattice spacing keeping the dimensionless quantity  $mr_0 = 8.4$  fixed. In Fig. 5, we plot the



**Fig. 3** The spectrum of  $D_W D_W^\dagger$ . The lattice setup is the same as Fig. 2.



**Fig. 4** The amplitude of the lowest eigenstate of  $D_W^\dagger D_W$  at  $r_0 = 24a$  and  $ma = 0.35$  (left) and that of  $D_W D_W^\dagger$  (right). The color gradation shows the local chirality.

relative ratio of the first eigenvalue,

$$\Delta\epsilon_j := \frac{|E_j| - |E_j^{\text{con.}}|}{|E_j^{\text{con.}}|}, \quad (43)$$

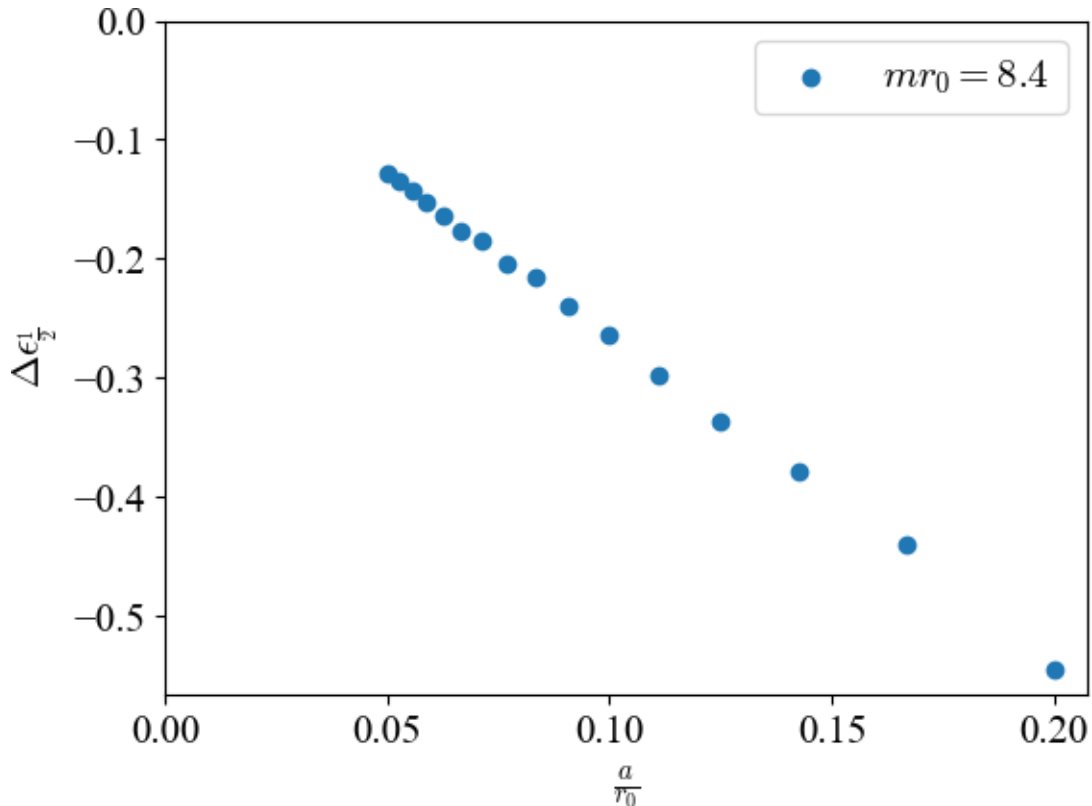


**Fig. 5** The relative deviation of the eigenvalue  $E_{1/2}$  as a function of the lattice spacing  $a$  with  $mr_0 = 8.4$ .

where  $E_j^{\text{con.}}$  is the corresponding continuum prediction obtained by numerically solving Eq. (26). We can see that our lattice values are linearly approaching the continuum limit with the lattice spacing  $a$ .

In Fig. 6, we plot  $r_0|E_{1/2}|$  with a fixed lattice spacing  $ma = 0.35$ , as a function of  $r_0/a$ . The lattice results in lower triangle symbols are consistent with the continuum prediction given by the solid curve, which is

$$1 + \frac{1}{2mr_0} + O(1/(mr_0)^2),$$

in the large- $mr_0$  expansion. Note that the finite volume correction is not an exponential but a power function of  $r_0$ , since the propagating fermion at the edge is massless.

Finally let us examine the rotational symmetry in the continuum limit. The three plots in Fig. 7 show the same eigenfunction with  $j = 1/2$  with three different lattice spacings

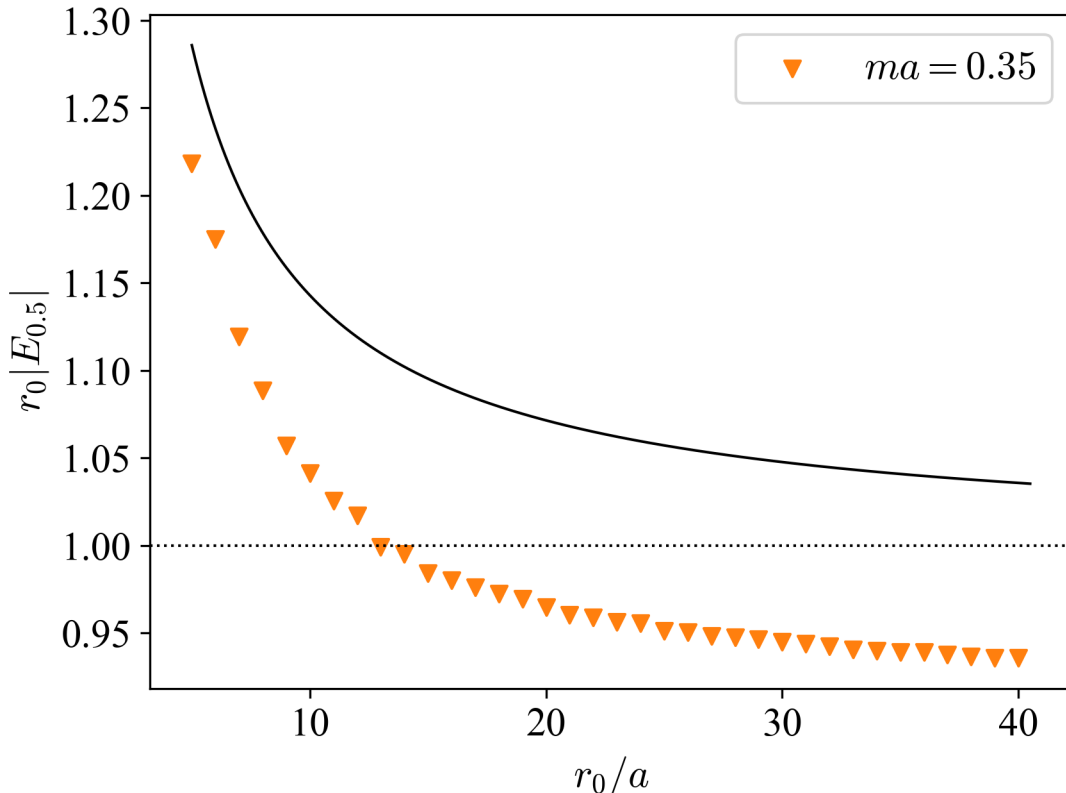


**Fig. 6** The finite volume effect on the eigenvalue of the lowest mode as a function of the radius of the sphere at  $ma = 0.35$ . The solid line represents the continuum prediction  $Er_0 = 1 + 1/2mr_0$ .

$a/r_0 = 1/16, 1/24$  and  $1/32$ . The finer the lattice spacing, the better the rotational symmetry looks. The symmetry can be quantified by taking the standard deviation  $\sigma$  of the amplitude peaks at the nearest-neighbor points to the domain-wall  $r = r_0$  normalized by their average  $\mu$  as presented in Fig. 8. The result is not monotonic but still shows a reasonable convergence to zero in the  $a \rightarrow 0$  limit. This supports that our digitized surface is a good regularization of the  $2D$  sphere.

The above numerical evidence in the free case shows that we can formulate a single Weyl fermion by this single curved domain-wall fermion on a square lattice. In the large- $mr_0$  limit, the finite volume effect is suppressed by  $1/mr_0$  and the chirality becomes exact. But below we will see that the system shows a nontrivial behavior when a gauge field is turned on.

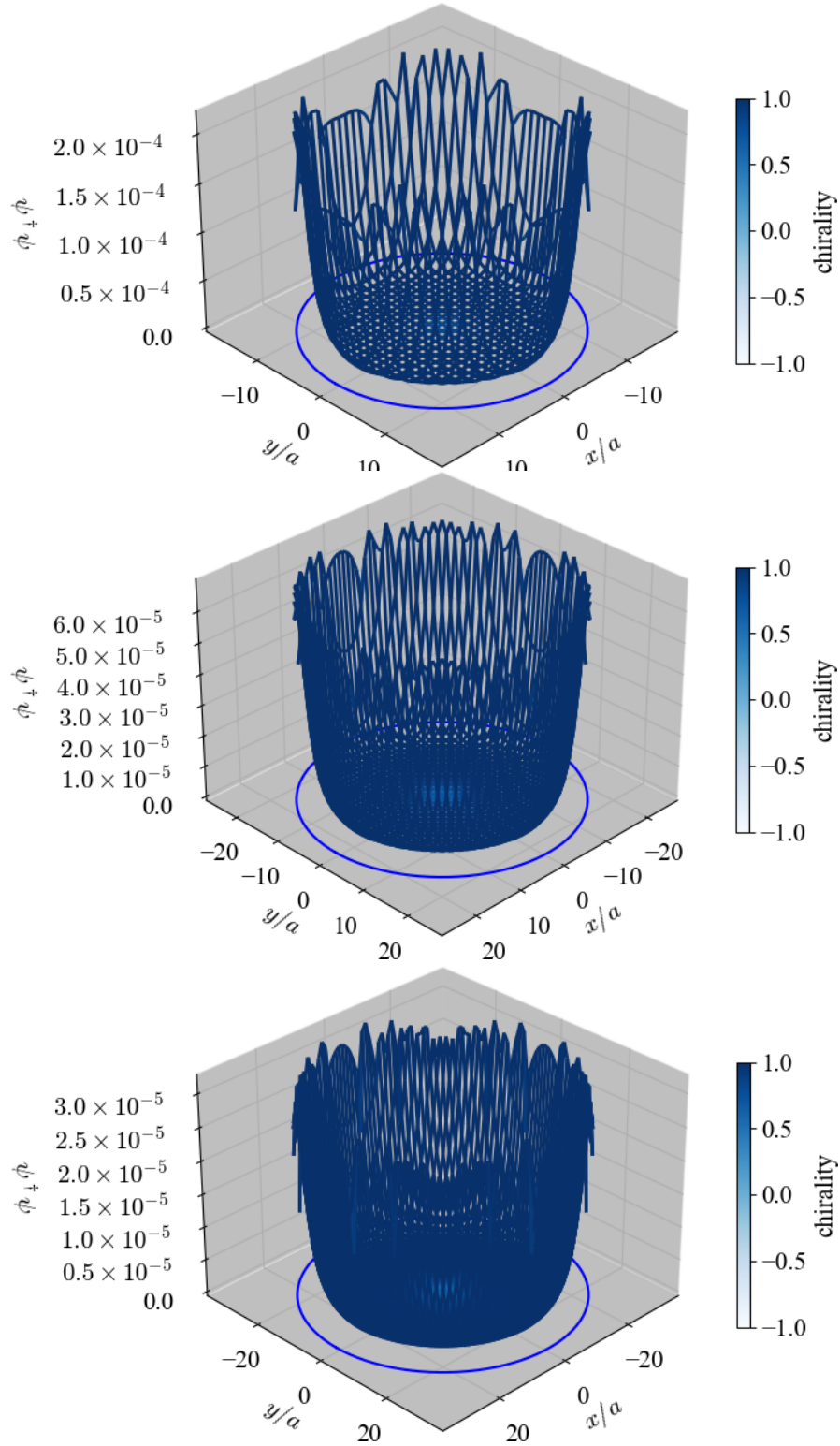


**Fig. 7** (Top) The amplitude of the lowest eigenstate of  $D_W^\dagger D_W$  at  $mr_0 = 8.4$  and  $a/r_0 = 1/16$ . (Middle) That at  $a/r_0 = 1/24$ . (Bottom) That at  $a/r_0 = 1/32$ .



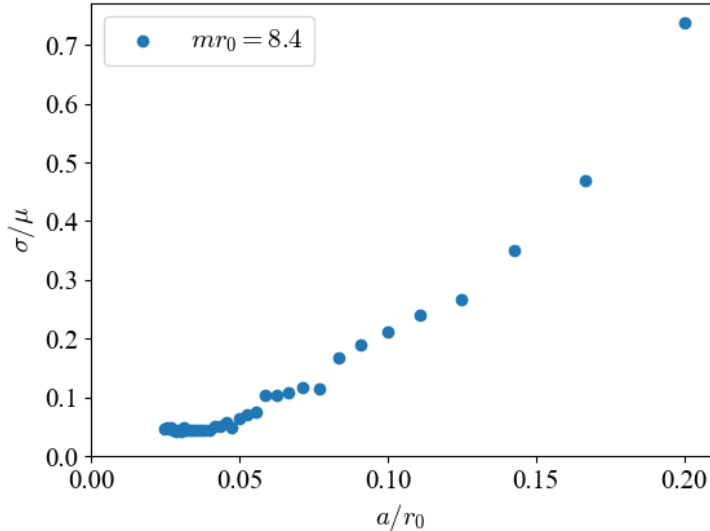


**Fig. 8** The standard deviation  $\sigma$  divided by the average  $\mu$  of the peaks as a function of the lattice spacing  $a$  with  $mr_0 = 8.4$ .

#### 4 With nontrivial $U(1)$ gauge fields

Next we set nontrivial  $U(1)$  gauge link variables,

$$U_j(x) = \exp\left(i \int_x^{x+\hat{j}} A_j(x') dx'^j\right), \quad (44)$$

where the vector potential  $A_j(x)$  is defined in Eq. (15). The covariant difference operator in the Wilson Dirac operator acts as

$$(\nabla_j \psi)_x = U_j(x) \psi_{x+\hat{j}} - \psi_x. \quad (45)$$

With these link variables, the Dirac string has no physical effect. In other words, the singularity of the continuum gauge field is automatically canceled by the multivaluedness of the  $U(1)$  link variables. To confirm this, let us compare the values of the two plaquettes  $p_+$  and  $p_-$  in the  $x$ - $y$  plane whose centers are located at  $x_+ = (0, 0, 1/2)$  and  $x_- = (0, 0, -1/2)$ , respectively. If the Dirac string is physical, the plaquette values should be asymmetric since the string intersects the plaquette at  $x_-$  but does not for the one at  $x_+$ . But this is not true:

by a direct computation, we obtain the symmetric result:

$$\begin{aligned}
p_{\pm} &= \exp \left[ i \int_{-1/2}^{1/2} dx A_1(x, -1/2, \pm 1/2) + i \int_{-1/2}^{1/2} dy A_2(1/2, y, \pm 1/2) \right. \\
&\quad \left. - i \int_{-1/2}^{1/2} dx A_1(x, 1/2, \pm 1/2) - i \int_{-1/2}^{1/2} dy A_2(-1/2, y, \pm 1/2) \right] \\
&= \exp(\pm \pi i n / 3),
\end{aligned} \tag{46}$$

which indicates that the magnetic flux from the monopole penetrating the two plaquettes at  $x_{\pm}$  is the same. On this lattice, the total magnetic flux from the monopole is nonzero, which allows violation of the Bianchi identity in the continuum limit.

In Fig. 9, we plot the eigenvalue spectrum of  $D_W^{\dagger} D_W$  with the monopole charge  $n = 1$  (top panel) and that with  $n = -1$  (bottom). The lattice setup is the same as Fig. 2. For  $n = +1$ , the lattice result is consistent with the continuum prediction marked by cross symbols. The low-lying modes with  $r_0|E| < mr_0$  have  $\sim +1$  chirality as the color gradation indicates. For  $n = -1$ , however, we find one near-zero mode with the opposite chirality  $\sigma_r = -1$ , which does not exist in the continuum analysis.

The amplitude of the oppositely chiral near-zero mode at the  $z = 1/2$  slice is plotted in Fig. 10. This mode is not located at the domain-wall but localized at the center where the monopole sits.

What is the origin of the new center-localized zero mode with the opposite chirality? In fact, in our previous work [37], we observed a similar phenomenon in the four-spinor system where a zero Dirac spinor mode appears in the vicinity of the monopole. Our microscopic analysis revealed that the additive mass renormalization from the Wilson term becomes strong enough at the singularity of the gauge field to flip the sign of the effective mass, which creates another small but finite domain-wall near the origin. This dynamically created domain-wall captures one edge-localized zero mode (of the electron), which explains why the monopole becomes dyon in topological insulators [39].

In the top panel of Fig. 11, we present the distribution in the  $z = 1/2$  slice of the effective mass defined by

$$M_{\text{eff}}(x) = \frac{\phi_0^{\dagger}(x) \left[ \sum_{i=1}^3 \frac{1}{2a} \nabla_i \nabla_i^{\dagger} - m \right] \phi_0(x)}{\phi_0^{\dagger}(x) \phi_0(x)}, \tag{47}$$

where  $\phi_0$  denotes the center-localized zero mode with  $n = -1$ . We can see that an island of the positive mass region whose edge is another domain-wall is created. For comparison, we also plot the same quantity but with the lowest eigenmode with  $n = 0$  in the bottom panel

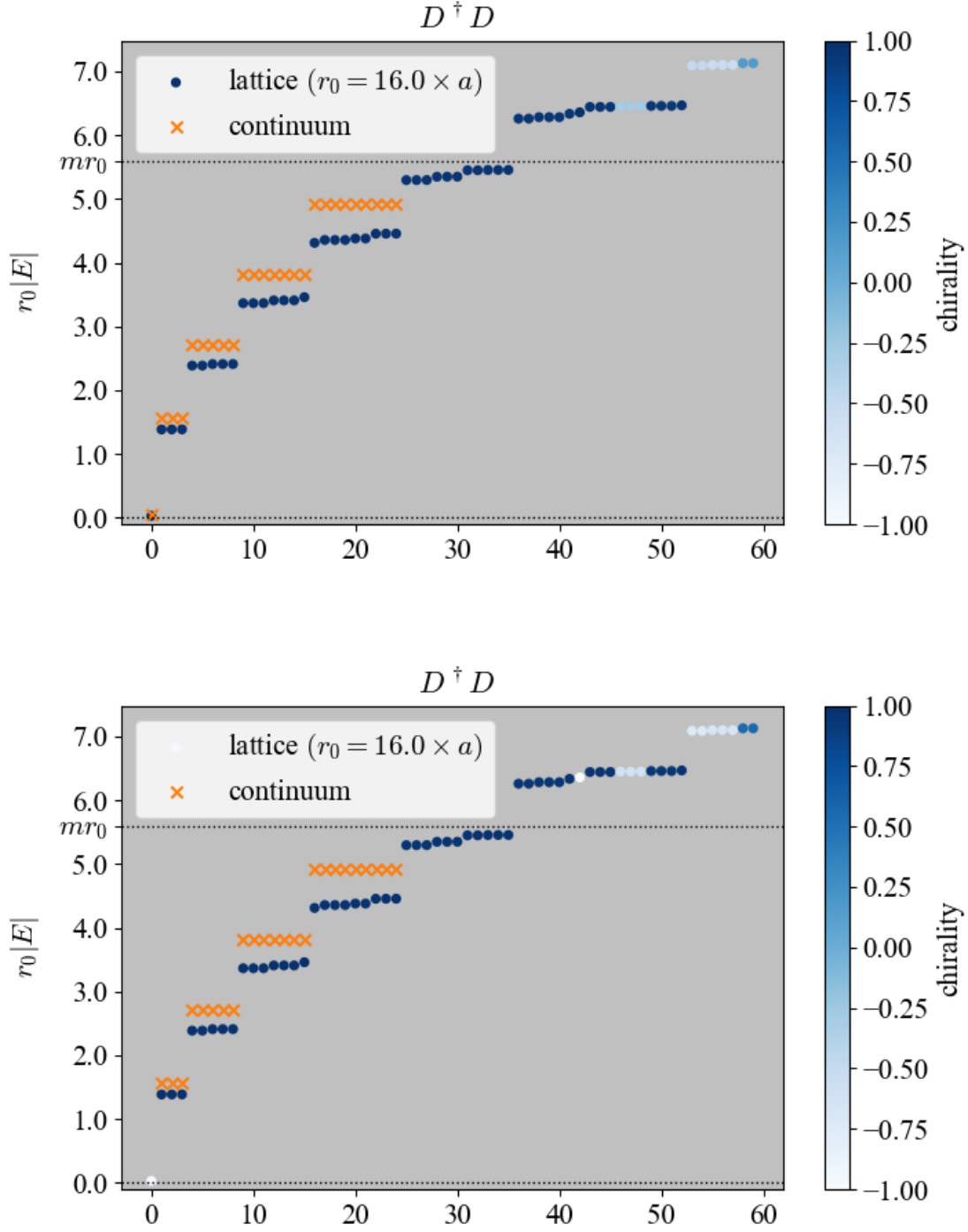


**Fig. 9** (Top) The eigenvalue spectrum of  $D_W^\dagger D_W$  with the monopole charge  $n = 1$ . Other lattice setup is the same as Fig. 2. (Bottom) The same but with  $n = -1$ . We can see a near-zero mode, which does not exist in the continuum prediction.

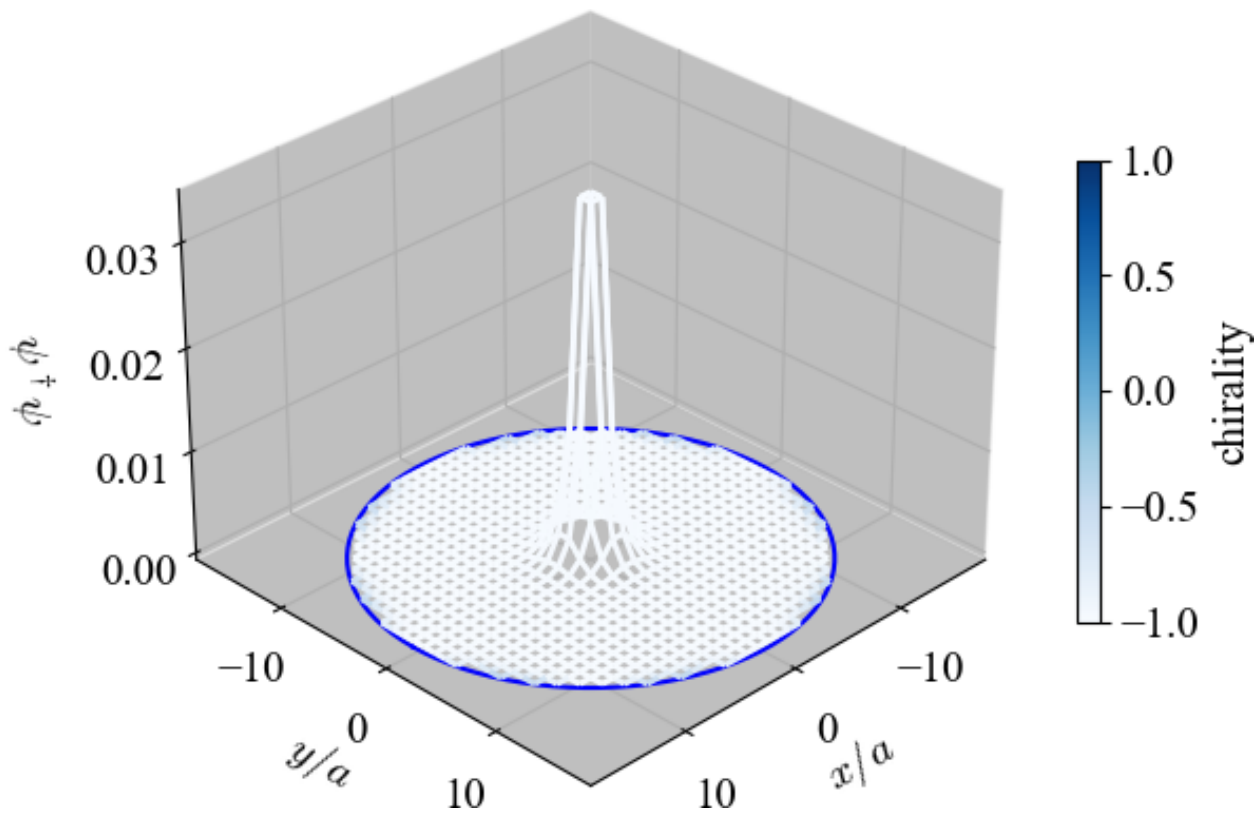


**Fig. 10** The amplitude of the zero mode of  $D_W^\dagger D_W$  at  $r_0 = 16a$ ,  $ma = 0.35$  and  $n = -1$ .

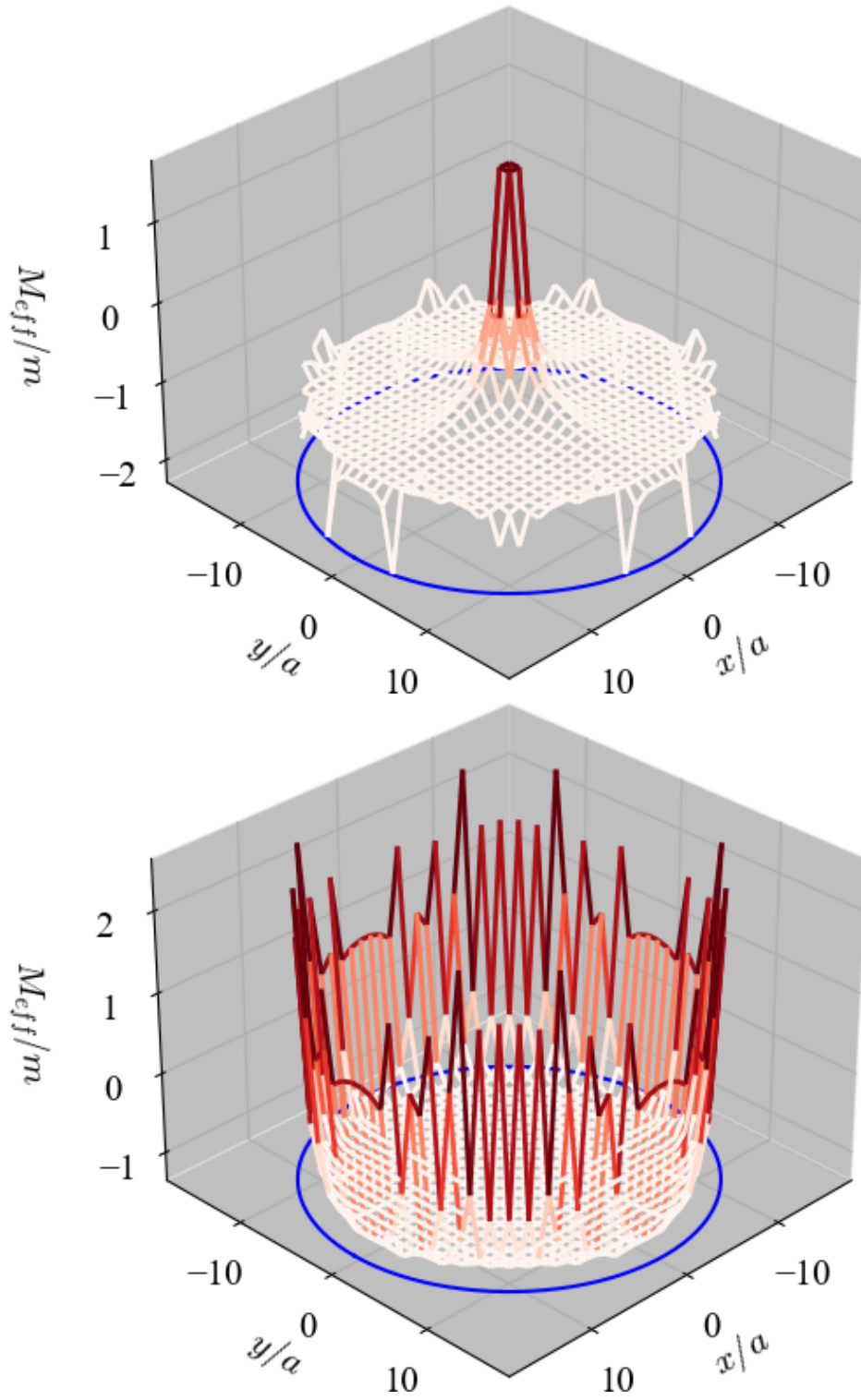
of Fig. 11, where the mass is negative everywhere except for the edge  $r = r_0$ . Thus, we can identify the center-localized zero mode as the edge mode of the new domain-wall near the monopole.

Figure 12 shows the eigenvalue distribution of  $D_W D_W^\dagger$ . A similar center-localized mode with positive chirality, which is opposite to that localized at  $r = r_0$  appears when  $n = +1$ .

The appearance of another domain-wall and the opposite chiral zero mode on it may indicate that the low-energy theory is not a simple chiral theory with a single Weyl fermion on a single domain-wall but a nontrivial vectorlike theory on the two domain-walls.

## 5 How to avoid opposite chiral modes

In this section we show in continuum analysis that the center-localized mode is stable against perturbation of the background gauge and gravity field since it is topologically protected. It is, therefore, crucial for constructing a chiral gauge theory in this setup, to find a formulation which eliminates such oppositely chiral zero modes.



**Fig. 11** (Top) The effective mass of the zero mode at  $n = -1$ . (Bottom) That of the lowest mode at  $n = 0$ . The red-white color gradation expresses the sign of the effective mass.

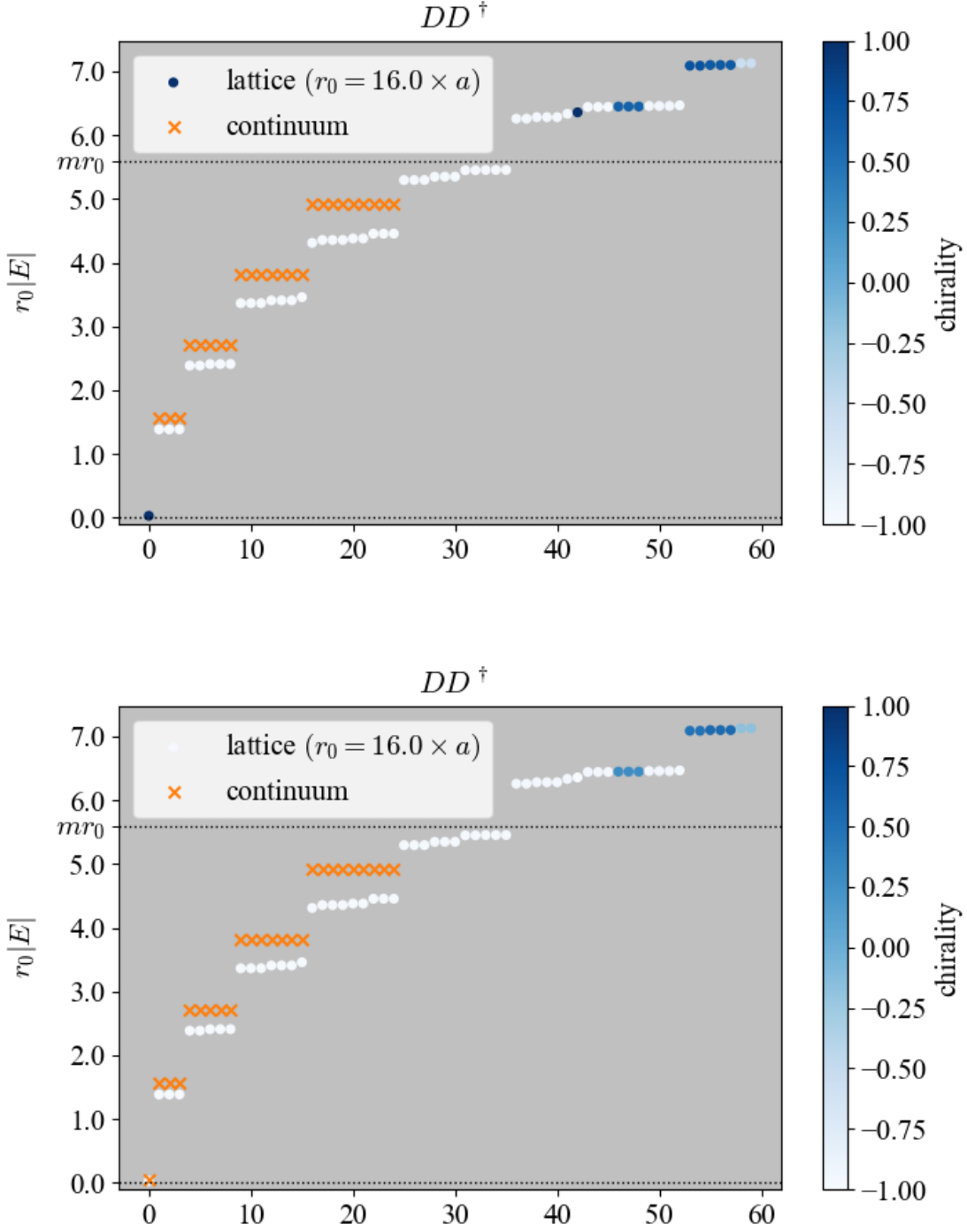


**Fig. 12** (Top) The eigenvalue spectrum of  $D_W D_W^\dagger$  with the monopole charge  $n = 1$ . Otherwise, the lattice setup is the same as Fig. 2. (Bottom) The same but with  $n = -1$ .

In order to make the problem explicit, let us consider a Hermitian operator in continuum

$$\hat{D} := \begin{pmatrix} 0 & D^\dagger \\ D & 0 \end{pmatrix}, \quad (48)$$

where the domain-wall Dirac operator  $D$  is defined as per Eq. (2) but with two domain-walls:

$$m(x) = \begin{cases} -m & \text{for } r_1 \leq |x| \leq r_0 \\ +M & \text{otherwise} \end{cases}, \quad (49)$$

where we assume that  $r_1$  is put in the vicinity of the monopole at the inverse of the cutoff scale.

In the  $M \rightarrow +\infty$  limit, the edge-localized states are the eigenmode of

$$\gamma := \sigma_3 \otimes \sigma_r. \quad (50)$$

The positive  $\gamma$  modes are located at the outer domain-wall at  $r = r_0$ , whereas the negative  $\gamma$  modes are at  $r = r_1$ . At the outer domain-wall, the Dirac operator acts as the  $2D$  massless operator Eq. (17) and the same is true for  $r = r_1$  but with different scale:

$$\bar{D}^{S^2} = \frac{1}{r_1} \left[ \sigma^i \left( L_i + n \frac{x_i}{2r} \right) + 1 \right]. \quad (51)$$

It is not difficult to see that the two massless Dirac operator  $D^{S^2}$  at  $r = r_0$  and  $\bar{D}^{S^2}$  at  $r = r_1$  share the same index:

$$\text{Ind} D^{S^2} = \text{Ind} \bar{D}^{S^2} = \frac{1}{4\pi} \int_{S^2} d^2x \epsilon^{\mu\nu} F_{\mu\nu} = n. \quad (52)$$

Namely, the existence of the zero modes at the two spherical domain-walls is topologically guaranteed by the AS index on them. For  $n > 0$ , the two zero modes with  $\sigma_r = \text{sgn}(n)$  appear for  $D$  on the  $r = r_0$  domain-wall and another for  $D^\dagger$  is localized at  $r = r_1$ . For  $n < 0$ , there are also two zero modes but the roles of the  $r_0$  and  $r_1$  are flipped.

The above equivalence  $\text{Ind} D^{S^2} = \text{Ind} \bar{D}^{S^2}$  is a consequence of cobordism invariance of the AS index. Since the two spheres at  $r = r_0$  and  $r = r_1$  share the same bulk region in  $r_1 < r < r_0$ , they are cobordant and must have the same index.

Therefore, the opposite chiral zero modes are as stable as those localized at the edge  $r = r_0$  against any perturbative deformation of the configuration. Their existence in this continuum analysis looks like a serious obstacle in constructing a chiral gauge theory. The situation is apparently the same as the flat two domain-wall system where it is difficult to decouple the unwanted opposite chiral modes from the theory. Some times ago a promising

proposal was made, to use the Yang-Mills gradient flow to turn off the gauge interaction for one of the chiral modes in the two domain-wall fermion system [11, 12]. However it was pointed out in Ref. [13] (see also related works [14–17]) that a topologically nontrivial gauge background cannot eliminate the zero modes that originated from the AS index. This is also a consequence of the cobordism invariance of the index.

Note, however, that the situation on the lattice is not exactly the same as the continuum analysis above. First, the inner domain-wall is not fixed but can appear only with singular gauge field configuration. Second, the center-localized mode is effectively a zero-dimensional object, having no  $\theta$  and  $\phi$  dependence on the small sphere, which is isolated from the bulk modes. Taking these differences from the flat two-domain-wall case into account, we would like to propose two ideas which may be useful to avoid appearance of the opposite chiral modes.

One is to impose the admissibility condition [44] or a smoothness condition for every plaquette on the lattice. Under this condition, the only admissible link gauge fields, satisfying

$$\|1 - P_{ij}(x)\| < \epsilon, \quad (53)$$

with some small real number  $\epsilon$  are taken to construct the theory. Then, singular configurations are not allowed in the theory. In the continuum limit, the condition is equivalent to imposing the Bianchi identity.

Under the admissibility condition, we cannot put a monopole on the lattice. If  $\epsilon$  is small enough, we will be able to limit the additive mass renormalization through the Wilson term and avoid dynamical creation of the domain-walls. However, this would restrict the surface theory to be fixed in a topologically trivial sector where the instanton number is forced to be zero. By enlarging the gauge symmetry, which is a well-known prescription by 't Hooft and Polyakov [45, 46], this fixing topology problem may be circumvented but the discussion is beyond the scope of this work.

The second proposal is to resort to the so-called symmetric mass generation. Recently many studies [18–31] have discussed possibility of gapping out the edge-localized modes for special combinations of Weyl fermions by nontrivial interactions such as four-Fermi vertices, without breaking the chiral symmetry. This is possible only when their both perturbative and nonperturbative gauge anomalies are canceled. Since the unwanted center-localized modes in our system are essentially zero-dimensional, the analysis may be a lot easier than for those in general dimensions. Once the center-localized zero modes were gapped out, they would have an eigenvalue which scales as  $1/r_1$ , and we will be able to show that they are decoupled from the low-energy dynamics and the total system is essentially chiral.



## 6 Summary and discussion

In this work, we have investigated a Shamir lattice domain-wall fermion system with a single curved surface. We have embedded a  $2D$  spherical domain-wall into a  $3D$  flat square lattice ignoring fermion hopping to the outside of the domain-wall. Solving the Dirac equation of the  $3D$  negatively massive Wilson fermion in this system, we have examined the existence of massless chiral edge-localized modes and the gravity they feel through the induced spin connections.

In the free fermion theory with trivial gauge link variables, we have verified the existence of the edge-localized modes on the surface. Moreover, we have shown that these edge modes are almost chiral and massless. We have also identified the effect of the induced gravity as a gap in the Dirac eigenvalue spectrum. The continuum extrapolation and large volume limit are well under control, including recovery of the rotational symmetry. Our single domain-wall fermion system thus describes a single Weyl fermion in the low-energy limit.

With nontrivial  $U(1)$  gauge link variables, however, it has turned out that the system shows a dramatic change. With the magnetic monopole-like configuration, we have observed that a center-localized zero mode appears in the vicinity of the monopole, having the opposite chirality to that of the edge modes. This was not expected in the continuum analysis, under a condition where the eigenfunctions are smooth everywhere. We have found that the singularity of the gauge field creates another small but finite domain-wall via additive mass renormalization near the origin, which makes the massless zero mode localized at the wall.

We have discussed the stability of the dynamically created domain-wall and the center-localized zero mode on it and shown that they are topologically protected by the AS index theorem on the sphere. We have then made two proposals to avoid the appearance of these opposite chiral zero modes. One is to impose the admissibility condition, and another is the use of symmetric mass generation. The smallness of the domain-wall radius may help in the analysis of the center-localized mode as it is essentially a zero-dimensional object, which is greatly isolated from the massive bulk modes.

We thank S. Aoki, M. Furuta, S. Iso, D.B. Kaplan, Y. Kikukawa, M. Koshino, Y. Matsuki, S. Matsuo, T. Onogi, S. Yamaguchi, M. Yamashita and R. Yokokura for useful discussions. In particular, we thank Y. Kikukawa for his instruction to technical details on the symmetric mass generation. The work of SA was supported by JSPS KAKENHI Grant Number JP23KJ1459. The work of HF and NK was supported by JSPS KAKENHI Grant Number JP22H01219.

## References

- [1] David B. Kaplan, A method for simulating chiral fermions on the lattice, *Physics Letters B*, **288**(3), 342–347 (1992).
- [2] Yigal Shamir, Chiral fermions from lattice boundaries, *Nuclear Physics B*, **406**(1-2), 90–106 (Sep 1993).
- [3] Vadim Furman and Yigal Shamir, Axial symmetries in lattice qcd with kaplan fermions, *Nuclear Physics B*, **439**(1-2), 54–78 (Apr 1995).
- [4] Maarten F. L. Golterman, Karl Jansen, and David B. Kaplan, Chern-Simons currents and chiral fermions on the lattice, *Phys. Lett. B*, **301**, 219–223 (1993), hep-lat/9209003.
- [5] Karl Jansen, Domain wall fermions and chiral gauge theories, *Phys. Rept.*, **273**, 1–54 (1996), hep-lat/9410018.
- [6] David B. Kaplan and Martin Schmaltz, Domain wall fermions and the eta invariant, *Phys. Lett. B*, **368**, 44–52 (1996), hep-th/9510197.
- [7] Yoshio Kikukawa and Yoichi Nakayama, Gauge anomaly cancellations in  $SU(2)(L) \times U(1)(Y)$  electroweak theory on the lattice, *Nucl. Phys. B*, **597**, 519–536 (2001), hep-lat/0005015.
- [8] Herbert Neuberger, Exactly massless quarks on the lattice, *Phys. Lett. B*, **417**, 141–144 (1998), hep-lat/9707022.
- [9] Martin Luscher, Abelian chiral gauge theories on the lattice with exact gauge invariance, *Nucl. Phys. B*, **549**, 295–334 (1999), hep-lat/9811032.
- [10] Martin Luscher, Weyl fermions on the lattice and the nonAbelian gauge anomaly, *Nucl. Phys. B*, **568**, 162–179 (2000), hep-lat/9904009.
- [11] Dorota M. Grabowska and David B. Kaplan, Nonperturbative Regulator for Chiral Gauge Theories?, *Phys. Rev. Lett.*, **116**(21), 211602 (2016), arXiv:1511.03649.
- [12] Dorota M. Grabowska and David B. Kaplan, Chiral solution to the Ginsparg-Wilson equation, *Phys. Rev. D*, **94**(11), 114504 (2016), arXiv:1610.02151.
- [13] Ken-ichi Okumura and Hiroshi Suzuki, Fermion number anomaly with the fluffy mirror fermion, *PTEP*, **2016**(12), 123B07 (2016), arXiv:1608.02217.
- [14] Yu Hamada and Hikaru Kawai, Axial  $U(1)$  current in Grabowska and Kaplan’s formulation, *PTEP*, **2017**(6), 063B09 (2017), arXiv:1705.01317.
- [15] Hiroki Makino and Okuto Morikawa, Lorentz symmetry violation in the fermion number anomaly with the chiral overlap operator, *PTEP*, **2016**(12), 123B06 (2016), arXiv:1609.08376.
- [16] Hiroki Makino, Okuto Morikawa, and Hiroshi Suzuki, One-loop perturbative coupling of  $A$  and  $A_*$  through the chiral overlap operator, *PTEP*, **2017**(6), 063B08 (2017), arXiv:1704.04862.
- [17] Taichi Ago and Yoshio Kikukawa, On the infinite gradient-flow for the domain-wall formulation of chiral lattice gauge theories, *JHEP*, **03**, 044 (2020), arXiv:1911.10925.
- [18] Xiao-Gang Wen, A lattice non-perturbative definition of an  $SO(10)$  chiral gauge theory and its induced standard model, *Chin. Phys. Lett.*, **30**, 111101 (2013), arXiv:1305.1045.
- [19] Juven Wang and Xiao-Gang Wen, Nonperturbative regularization of (1+1)-dimensional anomaly-free chiral fermions and bosons: On the equivalence of anomaly matching conditions and boundary gapping rules, *Phys. Rev. B*, **107**(1), 014311 (2023), arXiv:1307.7480.
- [20] Yoshio Kikukawa, On the gauge invariant path-integral measure for the overlap Weyl fermions in  $\underline{16}$  of  $SO(10)$ , *PTEP*, **2019**(11), 113B03 (2019), arXiv:1710.11618.
- [21] Yoshio Kikukawa, Why is the mission impossible? – Decoupling the mirror Ginsparg-Wilson fermions in the lattice models for two-dimensional abelian chiral gauge theories, *PTEP*, **2019**(7), 073B02 (2019), arXiv:1710.11101.
- [22] Juven Wang and Xiao-Gang Wen, Nonperturbative definition of the standard models, *Phys. Rev. Res.*, **2**(2), 023356 (2020), arXiv:1809.11171.
- [23] Yi-Zhuang You, Yin-Chen He, Cenke Xu, and Ashvin Vishwanath, Symmetric fermion mass generation as deconfined quantum criticality, *Physical Review X*, **8**(1), 011026 (2018).
- [24] David Tong, Comments on symmetric mass generation in 2d and 4d, *JHEP*, **07**, 001 (2022), arXiv:2104.03997.
- [25] Meng Zeng, Zheng Zhu, Juven Wang, and Yi-Zhuang You, Symmetric Mass Generation in the 1+1 Dimensional Chiral Fermion 3-4-5-0 Model, *Phys. Rev. Lett.*, **128**(18), 185301 (2022), arXiv:2202.12355.
- [26] Juven Wang and Yi-Zhuang You, Symmetric Mass Generation, *Symmetry*, **14**(7), 1475 (2022), arXiv:2204.14271.
- [27] Da-Chuan Lu, Juven Wang, and Yi-Zhuang You, Definition and classification of Fermi surface anomalies, *Phys. Rev. B*, **109**(4), 045123 (2024), arXiv:2302.12731.
- [28] Yuxuan Guo and Yi-Zhuang You, Symmetric mass generation of Kähler-Dirac fermions from the perspective of symmetry-protected topological phases, *Phys. Rev. B*, **108**(11), 115139 (2023), arXiv:2306.17420.
- [29] Da-Chuan Lu, Meng Zeng, and Yi-Zhuang You, Green’s function zeros in Fermi surface symmetric mass generation, *Phys. Rev. B*, **108**(20), 205117 (2023), arXiv:2307.12223.
- [30] Zi Hong Liu et al., Disorder Operator and Rényi Entanglement Entropy of Symmetric Mass Generation, *Phys. Rev. Lett.*, **132**(15), 156503 (2024), arXiv:2308.07380.

- [31] Maarten Golterman and Yigal Shamir, Propagator Zeros and Lattice Chiral Gauge Theories, *Phys. Rev. Lett.*, **132**(8), 081903 (2024), arXiv:2311.12790.
- [32] Shoto Aoki and Hidenori Fukaya, Curved domain-wall fermions, *PTEP*, **2022**(6), 063B04 (2022), arXiv:2203.03782.
- [33] Shoto Aoki and Hidenori Fukaya, Curved domain-wall fermion and its anomaly inflow, *PTEP*, **2023**(3), 033B05 (2023), arXiv:2212.11583.
- [34] Shoto Aoki, Hidenori Fukaya, and Naoto Kan, A lattice regularization of Weyl fermions in a gravitational background, *PoS, LATTICE2023*, 371 (2024), arXiv:2401.05636.
- [35] David B. Kaplan, Chiral Gauge Theory at the Boundary between Topological Phases, *Phys. Rev. Lett.*, **132**(14), 141603 (2024), arXiv:2312.01494.
- [36] David B. Kaplan and Srimoyee Sen, Weyl Fermions on a Finite Lattice, *Phys. Rev. Lett.*, **132**(14), 141604 (2024), arXiv:2312.04012.
- [37] Shoto Aoki, Hidenori Fukaya, Naoto Kan, Mikito Koshino, and Yoshiyuki Matsuki, Magnetic monopole becomes dyon in topological insulators, *Phys. Rev. B*, **108**(15), 155104 (2023), arXiv:2304.13954.
- [38] Naoto Kan, Shoto Aoki, Hidenori Fukaya, Mikito Koshino, and Yoshiyuki Matsuki, A Microscopic study of Magnetic monopoles in Topological Insulators, *PoS, LATTICE2023*, 363 (2024), arXiv:2401.05804.
- [39] Edward Witten, Dyons of Charge  $e\theta/2\pi$ , *Phys. Lett. B*, **86**, 283–287 (1979).
- [40] Shoto Aoki, Study of Curved Domain-wall Fermions on a Lattice (4 2024), arXiv:2404.01002.
- [41] Tai Tsun Wu and Chen Ning Yang, Dirac Monopole Without Strings: Monopole Harmonics, *Nucl. Phys. B*, **107**, 365 (1976).
- [42] Shoto Aoki and Hidenori Fukaya, Chiral fermion on curved domain-wall, *PoS, LATTICE2021*, 535 (2022), arXiv:2111.11649.
- [43] M. F. Atiyah and I. M. Singer, The index of elliptic operators on compact manifolds, *Bull. Am. Math. Soc.*, **69**, 422–433 (1963).
- [44] M. Luscher, Topology of Lattice Gauge Fields, *Commun. Math. Phys.*, **85**, 39 (1982).
- [45] Gerard 't Hooft, Magnetic monopoles in unified gauge theories, *Nucl. Phys. B*, **79**, 276–284 (May 1974).
- [46] Alexander M Polyakov, Particle spectrum in quantum field theory, *JETP Lett.*, **20**, 194–195 (1974).